

A CROSS-CORRELATION ANALYSIS OF AGN AND GALAXIES USING VIRTUAL OBSERVATORY: DEPENDENCE ON VIRIAL MASS OF SUPER-MASSIVE BLACK HOLE

YUTAKA KOMIYA, YUJI SHIRASAKI, MASATOSHI OHISHI, AND YOSHIHIKO MIZUMOTO

Draft version June 20, 2021

ABSTRACT

We present results of the cross-correlation analysis between active galactic nuclei (AGNs) and galaxies at redshift 0.1–1. We obtain data of $\sim 10,000$ SDSS AGNs in which their virial masses with a super-massive black hole (SMBH) were estimated. The UKIDSS galaxy samples around the AGNs were obtained using the virtual observatory. The scale length of AGN-galaxy cross-correlation for all of the samples is measured to be $r_0 = 5.8_{-0.6}^{+0.8} h^{-1} \text{Mpc}$ (for the fixed slope parameter $\gamma = 1.8$). We also derived a dependence of r_0 on the BH mass, M_{BH} , and found an indication of an increasing trend of r_0 at $M_{\text{BH}} > 10^8 M_{\odot}$. It is suggested that the growth of SMBH is mainly driven by interactions with the surrounding environment for $M_{\text{BH}} > 10^8 M_{\odot}$. On the other hand, at $M_{\text{BH}} \lesssim 10^8 M_{\odot}$, we did not find the BH mass dependence. This would imply that, for less massive BHs, the mass growth process can be different from that for massive BHs.

Subject headings: quasars: general – virtual observatory tools – large-scale structure of universe – galaxies: active – astronomical data bases: miscellaneous

1. INTRODUCTION

It is thought that most galaxies harbor supermassive black holes (SMBHs) in their centers, and that gas accretion onto a SMBH is the energy source of active galactic nucleus (AGN) (e.g. Richstone et al. 1998; Ferrarese & Ford 2005). There are strong correlations between mass of a SMBH and observational properties of its host galaxy such as velocity dispersion and stellar mass of the bulge (e.g. Magorrian et al. 1998; Ferrarese & Merritt 2000).

Growth of the BH mass is strongly coupled to the evolution of the host galaxy, but the process of “co-evolution” is still unknown. It is thought that BHs grow by accretion of gas and/or merger of BHs, but the physical mechanisms of gas inflow toward central regions of galaxies and coalescence of binary BHs are not yet revealed. In the standard hierarchical structure formation framework, major mergers of galaxies should have played important roles for evolution of galaxies, growth of SMBHs, and AGN activity. Thus, investigating the clustering of the galaxies around AGNs is crucial to understand evolution of SMBHs and galaxies.

Recent large-scale surveys, such as the Sloan Digital Sky Survey (SDSS), provide observational sample over 100,000 AGNs (Schneider et al. 2010). The auto-correlation function of AGNs was studied using the SDSS sample (Shen et al. 2007, 2009; Ross et al. 2009). The clustering of galaxies around AGNs in the areas of deep surveys was also investigated by some authors (e.g. Coil et al. 2009; Mountrichas et al. 2009). They showed that the cross-correlation function between AGNs and galaxies is similar to the auto-correlation of luminous red quiescent galaxies. Hickox et al. (2009) found that radio selected AGNs are strongly clustered, and that infra-red selected AGNs are weakly clustered than optically selected AGNs. Recently, cross-correlation between AGNs and galaxies was studied using large samples. Donoso et al. (2010) computed cross-correlation between $\sim 14,000$ radio-loud AGNs at $z = 0.4\text{--}0.8$ and reference luminous galaxy sample, and compared the clustering amplitude of radio-galaxies with that of $\sim 7,000$ SDSS quasars.

They argued that radio-loud AGNs are clustered more strongly than radio-quiet ones. Krumpe et al. (2012) investigated clustering of galaxies around $\sim 3,000$ X-ray selected AGNs and $\sim 8,000$ optically selected AGNs at $z < 0.5$. No significant difference was found between X-ray selected and optically selected broad-line AGNs.

In order to understand interaction between growth of SMBHs and their surrounding environment, it is important to investigate dependence of clustering amplitude on physical properties of BHs. Shen et al. (2009) studied the dependence of the two-point auto-correlation function of quasars on luminosity, BH mass, color, and radio loudness, and found weak or no dependence on virial BH mass. The cross-correlation function between AGNs and galaxies will achieve smaller uncertainties in clustering measurement because it has many more pairs at a given separation compared with the auto-correlation function of AGNs. Donoso et al. (2010) found positive dependence of the cross-correlation amplitude on stellar mass M_* , but their sample is radio-loud AGNs within a narrow range of stellar mass ($10^{11} M_{\odot} < M_* < 10^{12} M_{\odot}$). There is no previous study to investigate dependence of the cross-correlation function between AGNs and galaxies on BH mass over a wide mass range.

In this study, we investigate dependence of clustering amplitude of galaxies around AGNs on the BH mass to reveal a relation between mass growth of SMBHs and large scale environment of their host galaxies. We have collected observational data of a large number of AGNs and galaxies by using the Japanese Virtual Observatory (JVO)¹, and computed the cross-correlation function between AGNs and galaxies. Thanks to the large sample covering a large area of the sky, we were able to perform the clustering analysis in a manner free from the cosmic variance. To investigate BH mass dependence over a wide mass range ($\gtrsim 2\text{dex}$), we also use the sample of less massive BHs by Greene & Ho (2007) in addition to the SDSS quasar catalog (Shen et al. 2011), as described

¹ <http://jvo.nao.ac.jp/portal/>

below.

Throughout this paper, we use the following cosmological parameters: $\Omega_M = 0.3$, $\Omega_\Lambda = 0.7$, $h = 0.7$. All magnitudes are given in the AB system. All of the distances are measured in comoving coordinates.

2. DATASETS

The AGN sample was extracted from two catalogs by Shen et al. (2011) and Greene & Ho (2007), both of which contain the estimated virial mass, M_{BH} , of the SMBHs. Shen et al. (2011) derived virial mass of BHs for 105,783 quasars in the SDSS DR7 quasar catalog (Schneider et al. 2010). About a half of their samples were uniformly selected by the criteria described in Richards et al. (2002) and the remaining samples were selected by a variety of earlier algorithms or serendipitous selections.

Greene & Ho (2007) derived BH masses for $\sim 8,500$ active galaxies at $z < 0.35$ based on SDSS DR4 spectra. They also analyzed spectra for objects classified as galaxies, not only quasars. They extracted the AGN components from spectra of galaxies, and estimated BH masses. Their catalog contains more objects than the sample of Shen et al. (2011) for $M_{\text{BH}} \lesssim 10^7 M_\odot$.

They both estimated virial mass of BHs by means of observed FWHM of the emission lines of $\text{H}\alpha$, $\text{H}\beta$ or Mg II and the continuum luminosity at the lines. Shen et al. (2011) used $\text{H}\beta$ estimates for $z < 0.7$ and Mg II estimates for $z \geq 0.7$ as a fiducial virial mass estimate but also gave estimates based on other lines in their catalog when the lines were detected. For the samples of Shen et al. (2011), we used their fiducial mass estimate in this paper. Greene & Ho (2007) used $\text{H}\alpha$ estimates. We have found that there is systematic difference of ~ 0.5 dex between the virial masses estimated in the two catalogs mainly because they used different parameter values in the virial mass estimator. Figure 1 shows estimated mass of 2,139 AGNs which are registered in the both catalogs. For the samples of Greene & Ho (2007), we have recomputed virial mass by means of the FWHM and luminosity in Greene & Ho (2007) with the parameter values in Shen et al. (2011) for $\text{H}\alpha$ line. For the recomputed virial mass, the systematic difference is decreased as shown in the bottom panel of Figure 1. The recomputed masses by means of the data of Greene & Ho (2007), however, are still ~ 0.2 dex smaller than the estimated masses in the catalog of Shen et al. (2011) on average. A half of this remaining systematic difference is because of that FWHM and luminosity values were derived from the $\text{H}\alpha$ line for Greene & Ho (2007) but from $\text{H}\beta$ line for Shen et al. (2011). The other half is because of that Greene & Ho (2007) measured luminosity and FWHM of the emission lines of the extracted AGN components but Shen et al. (2011) measured the lines without eliminating the host galaxy component from the spectra. However, this difference with ~ 0.2 dex do not change our main conclusions as shown later. For the AGNs registered in the both two catalogs, we use data in the catalog of Shen et al. (2011).

We used the UKIDSS DR8 Large Area Survey (LAS) catalog (Lawrence et al. 2012) for galaxy samples. For each AGN, UKIDSS K -band data are searched around the AGN coordinates within 1 degree. We selected AGN samples of $z > 0.1$ in order to analyse projected number density as a function of projected distance r_p within

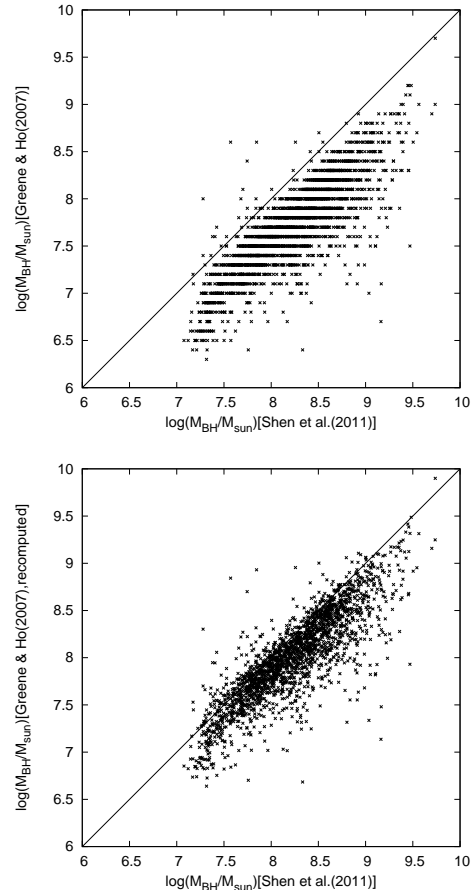


FIG. 1.— (Top panel) Black hole masses which is registered in the catalogs of Shen et al. (2011) and of Greene & Ho (2007). 2,139 objects are registered in the both catalogs. There is a mean offset of ~ 0.5 dex. (Bottom panel) For the data of Greene & Ho (2007), black hole masses were recomputed using the FWHM and luminosity in the catalog of Greene & Ho (2007) and the parameter values in the virial mass estimator in Shen et al. (2011). Offset and scatter decrease but a mean offset of ~ 0.2 dex remains. See text for detail.

$r_p \leq 7\text{Mpc}$ in the following. To obtain the data around the sample AGNs, we repeat to search galaxy data in the UKIDSS LAS catalog to the number of the sample AGNs. We obtained the data by accessing to the UKIDSS VO service through the JVO command line tools. By means of the VO tools we can recurrently access large data archives easily. To remove stars from the UKIDSS samples, we selected data for which the merged class flag equals to 1 (galaxies) or -3 (probable galaxies). We also removed data of poor quality which have the post-processing error quality bit larger than 255.

The limiting magnitude m_{limit} of the UKIDSS galaxy samples is estimated for each AGN sample, and the result is plotted in Figure 2. As can be seen from the figure, m_{limit} distributes around $19.7 - 20.3$. For each AGN, we also estimated threshold magnitude, m_{th} , below which detection efficiency for galaxies can be regarded as 100%. Figure 3 shows the absolute magnitude corresponding to m_{limit} and m_{th} at AGN redshift. The detailed definition of the m_{limit} and m_{th} is described in the next section.

To remove the data of poor sensitivity, we adapted selection criteria of $\rho_0 > 10^{-4}$ and $z < 1.0$, where ρ_0 is the average number density of galaxies detectable at the AGN redshift. ρ_0 was calculated by integrating the

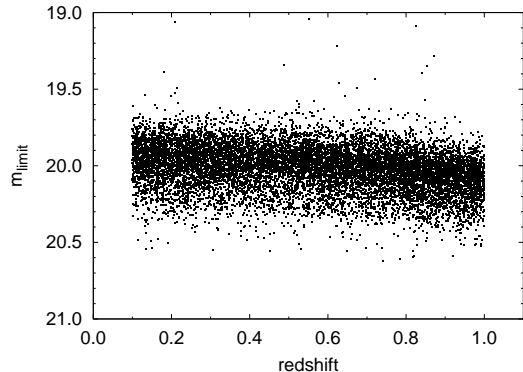


FIG. 2.— Distribution of the K -band limiting magnitude m_{limit} of the UKIDSS galaxies sample as a function of AGN redshift. Each point denote m_{limit} for the area around each AGN sample. 11,335 AGN samples of $z = 0.1 - 1.0$ are distributed in the survey area of UKIDSS LAS.

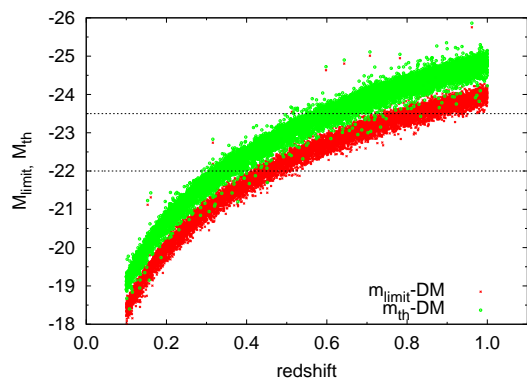


FIG. 3.— Distribution of the K -band absolute limiting magnitude $M_{\text{limit}} = m_{\text{limit}} - DM$ (red crosses) and absolute threshold magnitude $M_{\text{th}} = m_{\text{th}} - DM$ (green circles) of the UKIDSS galaxies around each AGN as a function of AGN redshift. Where DM is the distance modulus. m_{th} is a threshold magnitude defined in Equation (7), above which detection efficiency for galaxies becomes lower than 1.0. AGN samples are the same as Figure 2.

luminosity function upto the absolute magnitude corresponding to the apparent limiting magnitude m_{limit} as described in the next section and Shirasaki et al. (2011). Figure 4 shows the calculated ρ_0 as a function of AGN redshift. In the same figure the number densities of complete sample (blue) are also shown, and they are calculated by integrating the luminosity function upto the absolute magnitude corresponding to m_{th} . The combined AGN catalog, which are based on catalogs of Shen et al. (2011) and Greene & Ho (2007), lists 32,806 AGNs at redshift between 0.1 to 1.0. 11,335 objects are distributed in the survey area of UKIDSS LAS among them. In Figures 2 – 4, values for areas within 1 degree around these 11,335 AGNs are plotted. 10,482 AGNs are selected by the criterion of $\rho_0 > 10^{-4} \text{Mpc}^{-3}$ for m_{limit} .

To reduce the effect of foreground clusters which are accidentally located near the sample AGNs on the sky, we rejected samples with anomalous distribution of surrounding galaxy by the method described in Shirasaki et al. (2011). To reduce the effect of accidental alignment of the foreground cluster, we calculate the clustering coefficient, B_{QG} , around each AGN, which was defined as $\xi(r) = B_{QG} r^{-\gamma}$ (Barr et al. 2003), where $\xi(r)$ is the cross-correlation function. B_{QG} is calculated as

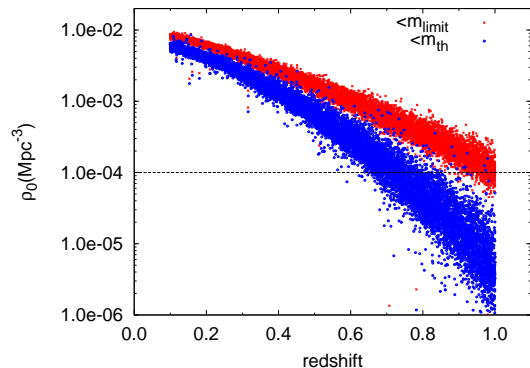


FIG. 4.— Distribution of the average number density ρ_0 of detectable galaxies ($< m_{\text{limit}}$, red crosses) and galaxies brighter than m_{th} (blue circles) at the AGN redshift for each AGN sample. Among the 11,335 AGN samples plotted in this figure, 10,482 AGNs with $\rho_0 > 10^{-4} \text{Mpc}^{-3}$ for detectable galaxies (red crosses above the dashed line) are use in the following analysis. For the analysis of the complete galaxy sample in Section 4.3, we use 6,107 AGNs with $\rho_0 > 10^{-4} \text{Mpc}^{-3}$ for galaxies brighter than m_{th} (blue circles above the dashed line).

$B_{QG} = \frac{3-\gamma}{2\pi C(\gamma)} \frac{N_{\text{total}} - N_{\text{bg}}}{\rho_0} (1\text{Mpc})^{\gamma-3}$, where N_{total} is the total number of observed galaxies at $r_p < 1$ Mpc, where r_p is a perpendicular distance, and N_{bg} is the expected background count at $r_p < 1\text{Mpc}$ (see Section 3 for the definition of ξ , r_p , γ , and $C(\gamma)$). We reject AGN samples with $|B_{QG}| > 10^4$ (30 times the clustering coefficient of the Abell class 0 objects). In addition, we select sample AGNs without the effect from the nearby cluster located in regions offset from the AGNs. We count number density $n(r_p)$ of UKIDSS galaxies for each circular region with $\Delta r_p = 0.2\text{Mpc}$ width around AGNs, and compute their statistical error. We adopt the following criteria: reduced χ^2 of the radial number density relative to the flat distribution is $\chi^2/(n-1) \leq 3$; the maximum deviation, σ_{max} , of the $n(r_p)$ is smaller than 5σ . In Section 4, we also show the results without these selection for comparison.

We also present result of analysis for the AGN subsample whose deviations of surface number density of UKIDSS sources is smaller than 1.5σ at limiting magnitude m_{limit} to check again the effect of foreground objects. Figure 5 shows the projected number density, $n_{7\text{Mpc}}$, of galaxies in the area around the AGN with an angular radius corresponding to 7Mpc (comoving) at the AGN redshift as a function of m_{limit} . Because the projected number density of the foreground or background galaxies is ~ 30 times larger than the galaxies in the host clusters even for the highly clustered region with $r_0 \sim 10\text{Mpc}$, this criterion rarely rejects sample AGNs with the real overdensities around them, but rejects AGNs located near the foreground clusters.

We used 9,394 AGNs, which were selected by criteria described in Shirasaki et al. (2011), in the following analysis. 8,060 AGNs were selected by the 1.5σ criterion for $n_{7\text{Mpc}}$. Figure 6 shows the distribution of the virial mass of the 9,394 SMBHs as a function of the redshift. 1,202 AGNs were extracted from the catalog of Greene & Ho (2007) (red crosses) and the others were from the catalog of Shen et al. (2011) (green circles). For the samples by Greene & Ho (2007), we plot the recomputed virial mass using the parameters of mass estimator in Shen et al. (2011). 3,749 objects among the samples from

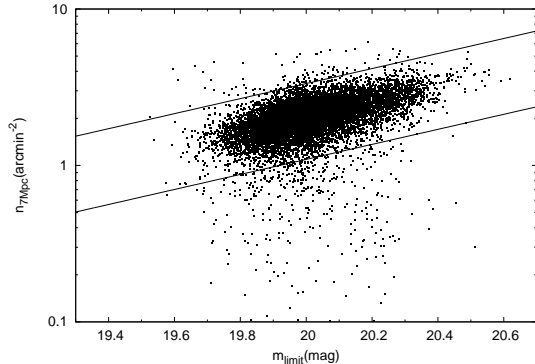


FIG. 5.— Distribution of the surface number density of galaxies around AGNs as a function of the K -band limiting magnitude. $n_{7\text{Mpc}}$ is the surface density of UKIDSS galaxies in the circular area around the AGN within an angular radius corresponding to 7Mpc(comoving) at the AGN redshift. We select AGN samples whose deviations of $\log n_{7\text{Mpc}}$ are less than 1.5σ (between the two solid lines) to reject effect of foreground clusters and bad quality regions of UKIDSS data. AGN samples are the same as Figure 2.

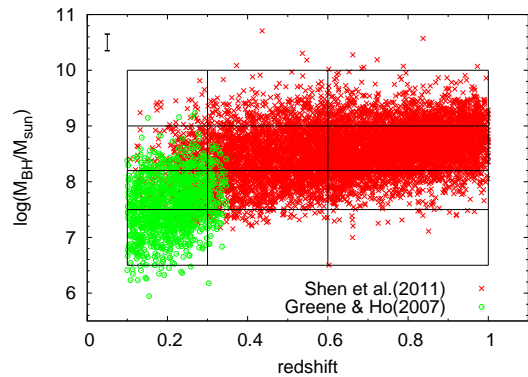


FIG. 6.— Distribution of 9,394 AGNs used in the following analysis in mass-redshift space. Red crosses and green circles denote samples by Shen et al. (2011) and Greene & Ho (2007), respectively. For the samples by Greene & Ho (2007), we plotted the recomputed virial mass by means of the parameter values of the mass estimator in Shen et al. (2011). The superposed grid indicates the sub-samples which we used to explore mass and redshift dependences. Bar at top left corner shows typical error for virial BH mass estimation.

Shen et al. (2011) had been identified by the uniform criteria of SDSS quasars (Richards et al. 2002). We also present the results of the clustering analysis for these sub-samples. We divided our sample into four mass bins of $\log(M_{\text{BH}}/M_{\odot}) = 6.5-7.2, 7.2-8.0, 8.0-9.0,$ and $9.0-10.0,$ and three redshift bins of $z = 0.1-0.3, 0.3-0.6, 0.6-1.0,$ to see mass and redshift dependences. The number, the averaged mass and the averaged redshift of AGN samples for each mass range and redshift range is listed in Table 1.

For $\sim 6\%$ of AGNs in our sample, radio counterparts were found in the FIRST source catalog (Schneider et al. 2010). The percentage of objects with radio counterparts is higher for AGNs with higher BH mass. The fraction of AGNs with radio counterpart is 14% at $M_{\text{BH}} > 10^9 M_{\odot}$. For $\sim 12\%$ of the sample AGNs, X-ray counterparts were found in the ROSAT catalog. The fraction of AGNs with X-ray detection is almost the same for all the BH mass ranges.

3. ANALYSIS METHOD

We have followed the method described in Shirasaki et al. (2011) for the cross-correlation analysis between AGNs and galaxies.

The cross-correlation function of AGNs and galaxies $\xi(r)$ can be expressed as an excess of number density of galaxies $\rho(r)$ relative to the average density ρ_0 at the AGN redshift.

$$\xi(r) = \frac{\rho(r)}{\rho_0} - 1, \quad (1)$$

where r represents the distance from an AGN.

In this analysis the redshift of galaxies are not measured, thus a projected cross correlation function $\omega(r_p)$ is calculated from projected number densities of galaxies $n(r_p)$:

$$\omega(r_p) = \frac{n(r_p) - n_{\text{bg}}}{\rho_0}, \quad (2)$$

where r_p represents projected distance from an AGN at the redshift, and n_{bg} represents the surface density of background/foreground galaxies.

3.1. Estimating the Average Density and the Limiting Magnitude

Estimation of ρ_0 is crucial for this analysis. However, we cannot estimate ρ_0 directly from the data itself since the information on the redshift is lacking. In this work, we estimated ρ_0 based on the luminosity function of galaxies obtained by previous studies (Cirasuolo et al. 2007; Gabasch et al. 2004, 2006; Kochanek et al. 2001; Montero-Dorta & Prada 2009). The luminosity function $\phi(M; z, \lambda)$ is parametrized as a function of redshift z and rest-frame wavelength λ as follows.

We use the Schechter function to represent the luminosity function,

$$\phi(M) = 0.4 \cdot \phi_* \cdot \ln(10) \cdot 10^{-0.4(M-M_*)(\alpha+1)} \cdot \exp[-10^{-0.4(M-M_*)}]. \quad (3)$$

In Figure 7, M_* and $\phi(M_0)$ derived from the fitting function obtained in the works by Cirasuolo et al. (2007); Gabasch et al. (2004, 2006); Kochanek et al. (2001); Montero-Dorta & Prada (2009) are plotted as a function of redshift for each rest-frame wavelength. M_0 is a reference magnitude where the luminosity function is normalized and parametrized as a function of redshift, and it is selected at a dimmer side of the M_* magnitude. Those data points are fitted with a 3rd degree polynomial function of redshift as shown in the Figure 7 as solid lines. The standard deviations of M_* and $\phi(M_0)$ from the fitted functions are 0.2 mag and 15%, respectively. For the parameter α , we used fixed values such as -1.1 for $\lambda < 400\text{nm}$, -1.25 for $400 \leq \lambda < 1000\text{nm}$, and -1.0 for $\lambda \geq 1000\text{nm}$.

As M_* and $\phi(M_0)$ at an arbitrary redshift for the eight wavelength bands can be calculated using the parametrization derived above, these parameters at an arbitrary wavelength are derived by interpolating them as a function of wavelength with a cubic spline method. In this way, we parametrized the luminosity function as function of redshift and rest-frame wavelength. We estimate ρ_0 by means of the Schechter function with the parameters at the AGN redshift and wavelength corresponding to the observed K band.

ρ_0 can be calculated by integrating $\phi(M; z, \lambda)$ to the absolute magnitude M at an AGN redshift corresponding

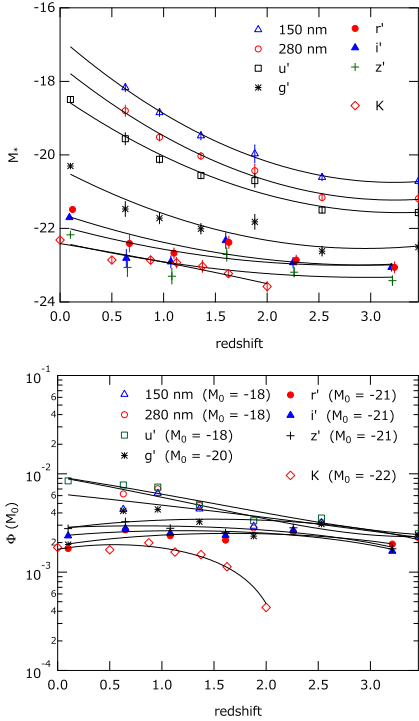


FIG. 7.— Parameters of the Schechter function derived by Cirasuolo et al. 2007 (K -band, $z \geq 0.5$), Gabasch et al. 2004 (150nm, 280nm, u' , and g' , $z \geq 0.6$) Gabasch et al. 2006 (r' , i' , and z' , $z \geq 0.6$) Kochanek et al. 2001 (K -band, $z = 0$) Montero-Dorta & Prada 2009 (u' , g' , r' , i' , and z' , $z = 0.1$). The solid lines represent fitting functions to parametrize M_* and $\Phi(M_0)$ as a function of redshift. *Top panel:* M_* for each rest-frame wavelength band. *Bottom panel:* Number densities $\Phi(M_0)$ at a reference magnitude M_0 . The reference magnitude M_0 for each wavelength band is -18 for 150 nm, 280 nm, and u' band, -20 for g' band, -21 for r' , i' , and z' band, and -22 for K band. to an apparent limiting magnitude m_{limit} ,

$$\rho_0 = \int_{m_{\text{low}} - DM(z)}^{m_{\text{limit}} - DM(z)} \phi(M; z, \lambda) dM, \quad (4)$$

where DM is the distance modulus and m_{low} is a lower boundary of the apparent magnitude.

As the limiting magnitude varies among the AGN samples, it was estimated from the measured magnitude distribution $N(m)$ as explained below. The observed magnitude distribution $N_{\text{obs}}(m)$ can be expressed as a multiplication of the *true* magnitude distribution $N_{\text{true}}(m)$ and the detection efficiency $DE(m)$:

$$N_{\text{obs}}(m) = N_{\text{true}}(m) \times DE(m). \quad (5)$$

We model $N_{\text{true}}(m)$ and $DE(m)$ as introduced in Shirasaki et al. (2011):

$$N_{\text{true}}(m) = \begin{cases} c \cdot 10^{a(m-m_b)} & (m < m_b) \\ c \cdot 10^{b(m-m_b)} & (m \geq m_b) \end{cases}, \quad (6)$$

$$DE(m) = \begin{cases} 1 & (m < m_{\text{th}}) \\ \exp(-(m - m_{\text{th}})^2 / \sigma_m^2) & (m \geq m_{\text{th}}) \end{cases}, \quad (7)$$

By fitting the model function of $N_{\text{obs}}(m)$ to the observed magnitude distribution, we obtained the model parameters a , b , c , m_b , m_{th} and σ_m for each area around an AGN sample. We determine ρ_0 as:

$$\rho_0 = \int_{m_{\text{low}} - DM}^{\infty} \phi(M; z, \lambda) DE(M + DM) dM \quad (8)$$

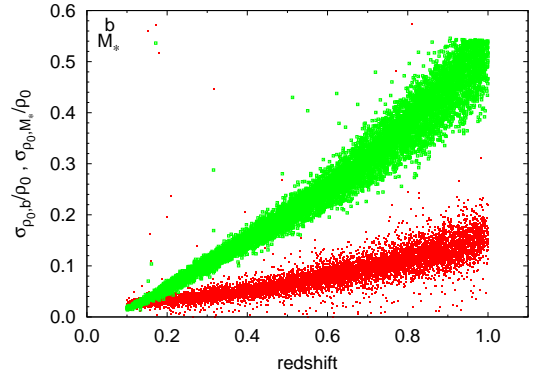


FIG. 8.— Fraction of uncertainty of ρ_0 originated from the uncertainty of the model parameter b (red filled square) and M_* (green open square) of the *true* magnitude distribution.

Equating the right-hand sides of Equation (4) and (8), m_{limit} is derived.

The uncertainty of ρ_0 determined as explained above is dominated with the uncertainties of the model parameters b and uncertainties of parametrization of the luminosity function, and they are taken into account as a systematic error in estimating the cross correlation length. We estimate the uncertainty of b as 0.04, which comes from the standard deviation of b calculated for each AGN sample. Considering the uncertainty of b , corresponding uncertainties of m_{th} and σ_m are estimated by comparing these fitting parameters obtained by fixing the b parameter to $b_{\text{best}} \pm 0.04$, where b_{best} is the best fitting parameter for the AGN sample. The uncertainty of ρ_0 originated from the uncertainties of m_{th} and σ_m (i.e. b) are calculated with error propagation. The uncertainty $\sigma_{\rho_0, b}$ are plotted as a function of redshift in Figure 8.

To evaluate the uncertainty of ρ_0 due to the uncertainties of parametrization of the luminosity function, we assumed uncertainties of M_* and $\phi(M_0)$ to be 0.2 mag and 15% respectively, which are the standard deviation of data points in Figure 7 from the fitting functions.

σ_{ρ_0, M_*} is the uncertainty of ρ_0 due to the uncertainty of M_* , and is plotted in Figure 8. The uncertainty of ρ_0 due to the uncertainty of $\phi(M_0)$ is independent from redshift and is constant value of $\sigma_{\rho_0, \phi(M_0)} = 0.15$. Then the total uncertainty of ρ_0 is calculated as:

$$\sigma_{\rho_0}^2 = \sigma_{\rho_0, b}^2 + \sigma_{\rho_0, M_*}^2 + \sigma_{\rho_0, \phi(M_0)}^2 \quad (9)$$

3.2. Cross Correlation

We assume the power-law form for the cross-correlation function,

$$\xi(r) = \left(\frac{r}{r_0} \right)^{-\gamma}, \quad (10)$$

where r_0 is a correlation length, and γ is a power-law index and fixed to 1.8, which is a canonical value measured by many other works. Then the projected cross-correlation function can be expressed as:

$$\begin{aligned} \omega(r_p) &= 2 \int_0^{\infty} \xi(r_p, \pi) d\pi = 2 \int_{r_p}^{\infty} \frac{r \xi(r)}{\sqrt{r^2 - r_p^2}} dr \\ &= r_p \left(\frac{r_0}{r_p} \right)^{\gamma} \frac{\Gamma(\frac{1}{2}) \Gamma(\frac{\gamma-1}{2})}{\Gamma(\frac{\gamma}{2})}, \quad (11) \end{aligned}$$

where π and r_p are distance along and perpendicular to the line of sight, respectively, and Γ is the Gamma function.

From equations(2) and (11), the projected number density of galaxies around an AGN can be modeled as:

$$n(r_p) = C(\gamma) \times \rho_0 \times r_p \left(\frac{r_0}{r_p} \right)^\gamma + n_{\text{bg}}, \quad (12)$$

where the term of the Gamma function is represented by $C(\gamma)$. By fitting this model function to the observed projected number density, we can derive the model parameters r_0 and n_{bg} . ρ_0 is determined by the method described in Section 3.1 Since the clustering signature for each AGN is too weak to derive the parameters individually, we applied this fitting to the averages of $n(r_p)$ and ρ_0 for a given AGN group,

$$\langle n(r_p) \rangle = C(\gamma) \times \langle \rho_0 \rangle \times r_p \left(\frac{r_0}{r_p} \right)^\gamma + \langle n_{\text{bg}} \rangle, \quad (13)$$

and derive r_0 and $\langle n_{\text{bg}} \rangle$. The uncertainty of r_0 is calculated as square root of square sum of the systematic error derived from the uncertainty of ρ_0 described in equation (9) and statistical error of 1σ by fitting $\langle n(r_p) \rangle$. It should be noted that the cross-correlation function obtained by this method is not an average for the AGN group, but an average weighted with ρ_0 . Thus the result is biased to the low- z and high-sensitivity samples.

4. RESULTS

By the analysis described above, we have estimated the scale length of AGN-galaxy cross correlation for the whole sample to be $r_0 = 5.8_{-0.6}^{+0.8} h^{-1} \text{Mpc}$. This is comparable with or slightly smaller than results of the previous studies of AGN-galaxy cross-correlation ($r_0 = 5.95 \pm 0.90 h^{-1} \text{Mpc}$ for X-ray AGNs at $z = 0.7-1.4$, (Coil et al. 2009); $6.98 \pm 0.6 h^{-1} \text{Mpc}$ for optical AGNs at $z < 1$, (Mountrichas et al. 2009); $r_0 = 6.0 \pm 0.5 h^{-1} \text{Mpc}$ for optical AGNs at $0.2 < z < 0.6$, (Padmanabhan et al. 2009)). Donoso et al. (2010) found $r_0 = 8.35 \pm 0.09$ for radio AGNs and $r_0 = 5.02 \pm 0.24 h^{-1} \text{Mpc}$ for optical AGNs at $z = 0.4-0.8$. Krumpel et al. (2012) derived that $r_0 = 6.91_{-0.18}^{+0.17} h^{-1} \text{Mpc}$ at $z = 0.16-0.36$ between SDSS AGNs and the SDSS main-galaxy sample and $r_0 = 7.21_{-0.22}^{+0.21} h^{-1} \text{Mpc}$ at $z = 0.36-0.5$ for SDSS AGNs and luminous red galaxies.

Now, we present the results of cross-correlation analysis adopted for the four mass ranges described in Figure 6 and Table 1, to see the dependence of the clustering amplitude on BH mass. Figures 9 and 10 show the measured projected number density $n(r_p)$ and projected cross-correlation function $\omega(r_p)$, respectively, for each mass range. Four panels represent results for the mass ranges of $\log(M_{\text{BH}}/M_\odot) = 9.0 - 10.0$ (top left), $8.2 - 9.0$ (top right), $7.5 - 8.2$ (bottom left), and $6.5 - 7.5$ (bottom right). The projected number density of the areas of each circular ring is plotted with the Poisson error bars. Solid lines denote least- χ^2 fitting by the power-law (Eq. 13). The fitting parameters are summarized in Table 1.

Figure 11 shows the scale length r_0 of cross-correlation as a function of virial mass of SMBHs. Error bars of r_0 denote square root of square sum of the systematic error calculated from σ_{ρ_0} described in Section 3.1 and

the statistical error of 1σ . We can see a trend that r_0 increases as mass increases for $M_{\text{BH}} > 10^8 M_\odot$. When we consider only the statistical error, the significance of difference of r_0 is 9.6σ for between $\log(M_{\text{BH}}/M_\odot) = 7.5 - 8.2$ bin and $8.2-9.0$ bin, and 3.4σ for between $8.2-9.0$ bin and $9.0-10.0$ bin. For $M_{\text{BH}} \lesssim 10^8 M_\odot$, we cannot see the significant mass dependence. These trends are also seen for the dataset grouped with finer mass ranges.

Figure 12 shows r_0 for AGN samples from the catalog of Shen et al. 2011 (green circles) which are identified by the uniform criteria of SDSS (Richards et al. 2002) and for samples of Greene & Ho 2007 (blue triangles). As seen in the figure, the mass dependences of both sub-samples are quite similar. We can see, however, a little offset between the results for the two sub-samples. This can be due to the systematic difference of the BH mass estimate with ~ 0.2 dex between the two catalogs as mentioned in Section 2.

We rejected sample AGNs with anomalous galaxy distribution around the AGNs, as described in the Section 2 to remove the effect from foreground objects. To see whether we are removing real clustering by this rejection, we present the results of the analysis done both with and without the selection, in Figure 13. The blue triangles show the results without any sample rejection. We cannot find significant clustering signal at $\log(M_{\text{BH}}/M_\odot) < 7.5$ for this analysis. The red squares are the fiducial results with the selection criteria described in Shirasaki et al. (2011). For green circles, we also reject AGN samples with extremely high or low projected number density ($n_{7\text{Mpc}}$) of galaxies around them.

The analysis without selection gives slightly smaller r_0 . This indicate that the clustering feature is weakened by foreground contamination for the analysis without sample rejection. The analysis with the $n_{7\text{Mpc}}$ criterion gives $r_0 = 6.3_{-0.6}^{+0.9} h^{-1} \text{Mpc}$ for the whole mass range. This is $\sim 0.5 h^{-1} \text{Mpc}$ larger than the result without the $n_{7\text{Mpc}}$ criterion. On the other hand, we see almost same relative mass dependence for the all three cases.

4.1. AGN Redshift

As seen in Figure 6, distribution of the BH mass in our sample depends on the redshift. This is because SMBHs with larger mass tend to be luminous and can be observed even at higher redshift. To see the dependence on the redshift, we divided the samples into three groups with redshift ranges of $z = 0.1-0.3$, $z = 0.3-0.6$, and $z = 0.6-1.0$. Figure 14 shows the estimated r_0 for the three redshift ranges and four mass ranges. As seen in the top panel of this figure, r_0 is not dependent on the redshift. Therefore, the increasing trend of r_0 seen in Figure 11 would not be due to the redshift bias. We could also see the mass dependence for the sub-samples of low redshift ($z = 0.1-0.3$, red squares) and intermediate redshift ($z = 0.3-0.6$, green circles). For higher redshift sample ($z = 0.6-1.0$), the estimated error is too large to see the dependence on BH mass. We summarize the estimated r_0 , $\langle \rho_0 \rangle$ and $\langle n_{\text{bg}} \rangle$ for the each mass range and redshift range in Table 1.

To remove the possible redshift bias, we also present the mass dependence for sub-samples with the normalized redshift distributions. We constructed sub-samples as follows: For redshift bins with $\Delta z = 0.1$, the selec-

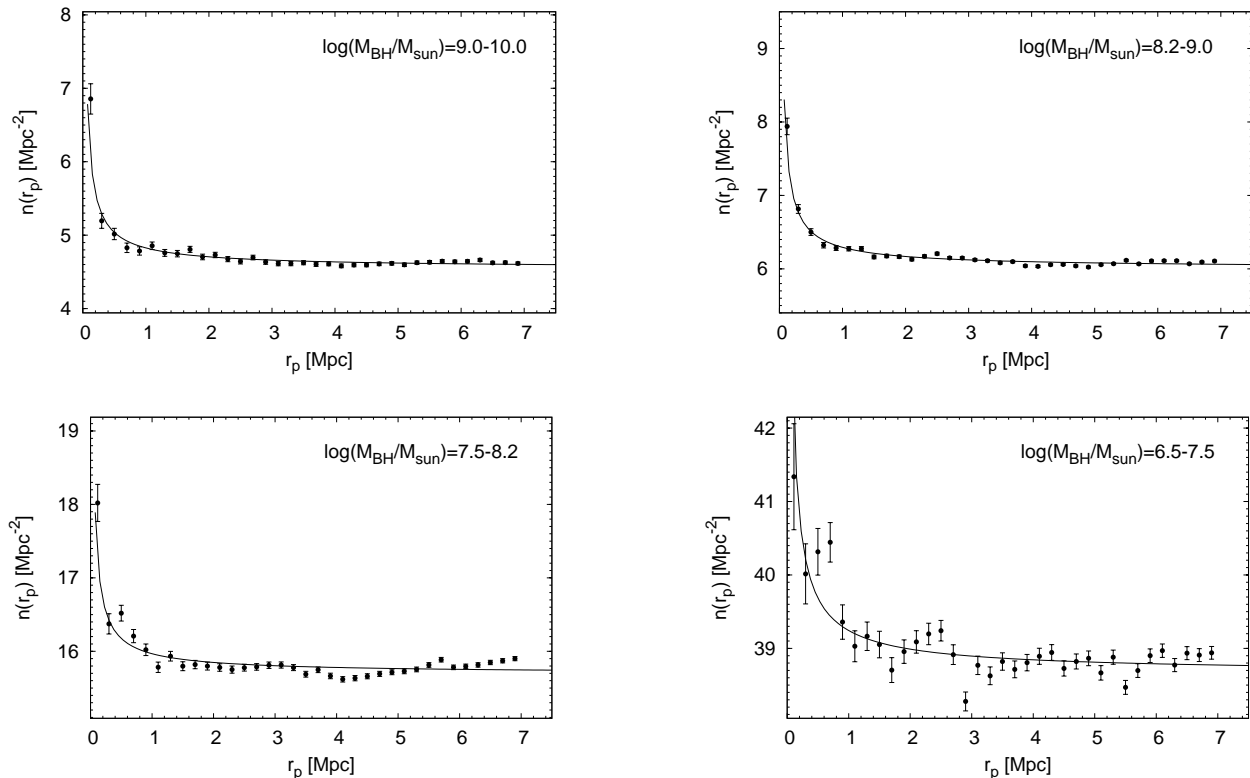


FIG. 9.— Projected number density of UKIDSS sources against projected distance from an AGN. Four panels show results for AGN samples in the four different mass ranges: $\log(M_{\text{BH}}/M_{\odot}) = 9.0 - 10.0$ (top left), $8.2 - 9.0$ (top right), $7.5 - 8.2$ (bottom left), and $6.5 - 7.5$ (bottom right). Poisson error bars of projected number density are attached. The solid lines denote least- χ^2 fit by the power function (Eq. 13).

tion probability is determined to give the same redshift distribution for the four mass ranges. We randomly selected AGN samples following the selection probability and constructed a sets of sub-samples. Figure 15 shows one example of the sub-sample. We constructed ten sets of sub-samples and measured r_0 for them. For these sub-samples, there is no correlation between redshift and BH mass.

Figure 16 shows the mass dependence of r_0 for the resampled AGNs with normalized redshift distribution. We plot medians of the ten sets of sub-samples as green circles. Error bars show maximum and minimum values for the ten sets. The resampled AGNs also show similar mass dependence as Figure 11. Large mass SMBHs show strong clustering amplitude at $M_{\text{BH}} > 10^8 M_{\odot}$. The clustering amplitude for AGNs with $\log(M_{\text{BH}}/M_{\odot}) = 6.5 - 7.5$ and $7.5 - 8.2$ is the almost same although the error bars are very large. The relative mass dependence for the sub-samples is free from redshift bias since the sub-samples for the four mass ranges have the same redshift distribution. We note that there is neither correlation between BH mass and luminosity for these sub-samples. Therefore, the BH mass dependence is thought to be neither due to redshift bias nor to luminosity bias.

4.2. AGN Luminosity

We divided our sample into three luminosity range of $L_{5100} < 10^{44.5}\text{erg/s}$, $10^{44.5}\text{erg/s} \leq L_{5100} < 10^{44.8}\text{erg/s}$, and $10^{44.8}\text{erg/s} \leq L_{5100}$ to see luminosity dependence, where L_{5100} is the monochromatic continuum luminosity at rest-frame 5100Å. The top panel of Figure 17 shows

the dependence of r_0 on luminosity. We cannot find significant luminosity dependence for all the four mass ranges. On the other hand, we could see the mass dependence at $M_{\text{BH}} > 10^8 M_{\odot}$ for all three luminosity ranges, as seen in the bottom panel. Therefore, we can conclude that the BH mass dependence seen in Figure 11 is not due to the dependence on luminosity.

Shen et al. (2009) argued that the amplitude of AGN-AGN auto-correlation depends weakly on optical luminosity. Donoso et al. (2010) found that the clustering amplitude varies with radio-luminosity on scales less than ~ 1 Mpc but is almost independent on luminosity for the larger scale.

These results indicate that the clustering amplitude on large scale depends on mass of SMBH but weakly depends on luminosity.

4.3. Completeness and Luminosity of the Galaxy Sample

As described in Section 3.1, we correct incompleteness of the faint end of galaxy sample by estimating the detection efficiency $DE(m)$ based on the magnitude distribution of UKIDSS sample for each area around an AGN. There may be a criticism that the correction of the incompleteness of the galaxy sample is somehow biased to the luminosity of the galaxy sample. Figure 18 shows the cross correlation length calculated for a complete galaxy sample which consist of blight galaxies with $m < m_{\text{th}}$, where m_{th} is a threshold magnitude, below which $DE(m) = 1$ (see Eq. 7). For this analysis, ρ_0 is also recomputed by integrating the luminosity function

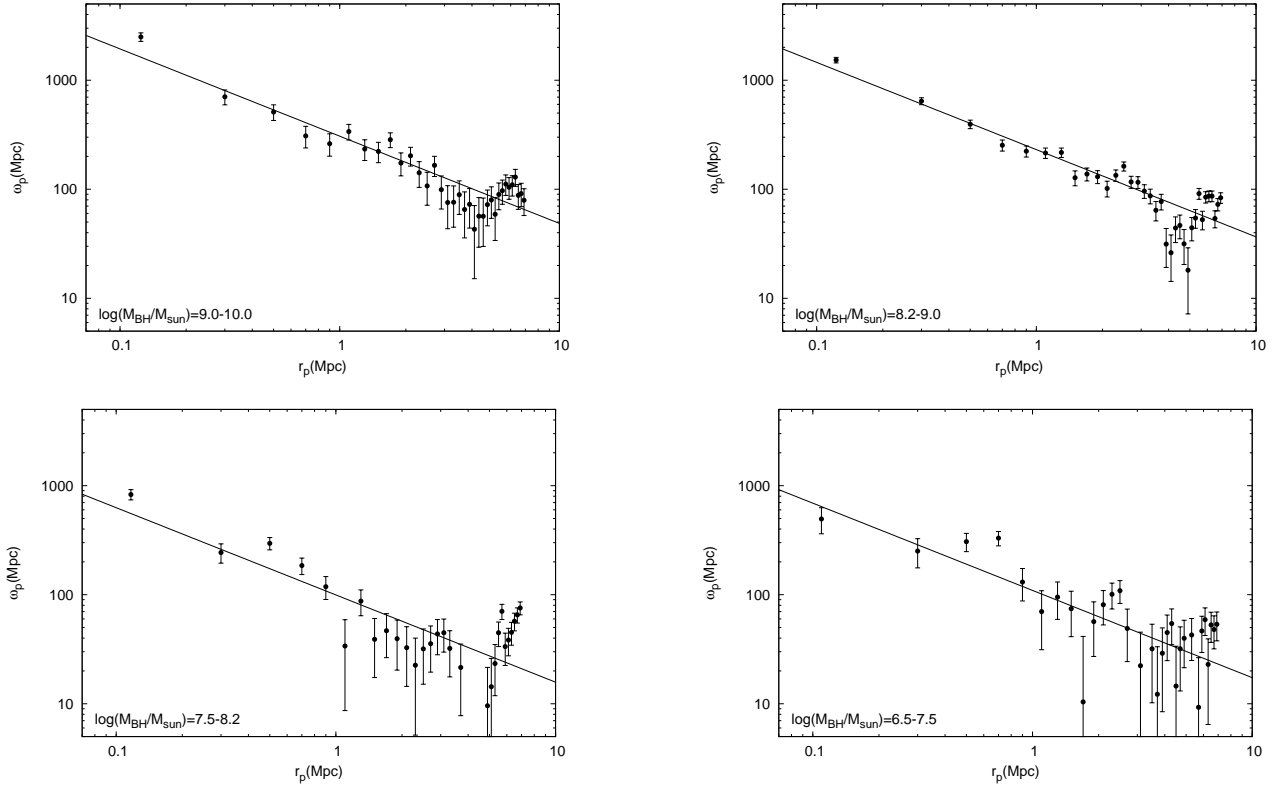


FIG. 10.— Projected cross correlation function of UKIDSS sources against projected distance from an AGN. Four panels show results for AGN samples in the four different mass ranges. Error bars show the uncertainty due to statistical error of projected number density. The solid lines denote least- χ^2 fit by the power function (Eq. 11).

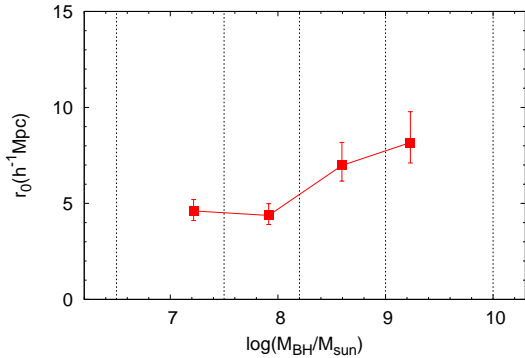


FIG. 11.— The scale length, r_0 , of the cross-correlation between AGNs and galaxies as a function of virial sum mass of SMBH. Error bars of r_0 denote square root of square sum of the systematic error derived from the uncertainty of the estimation of ρ_0 and statistical error of 1σ . Vertical dotted lines show boundaries of mass ranges.

upto m_{th} . This result also shows that the cross correlation increases above $M_{\text{BH}} \sim 10^8 M_{\odot}$. Therefore, the increasing trend is not due to the ambiguity that comes from using a incomplete galaxy sample.

It is known that brighter galaxies tend to cluster more strongly than dimmer galaxies. Thus it might be possible to explain the larger cross correlation length for more massive SMBH by the bias due to the galaxy brightness. Figure 19 shows the cross correlation length calculated for luminosity limited samples. We selected the luminosity limited galaxy samples which are defined as $M \equiv m - DM(z_{\text{AGN}}) < -22$, and $M < -23.5$ for each AGN, where $DM(z_{\text{AGN}})$ represents distance modulus for the AGN redshift. M is not absolute magnitude for fore-

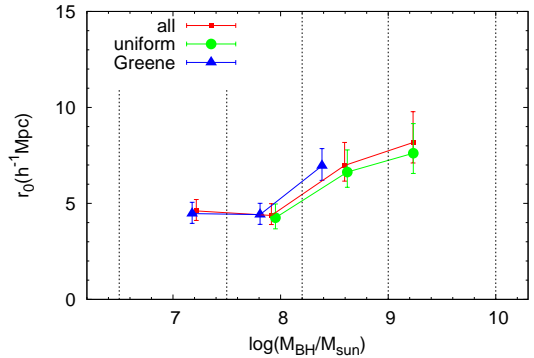


FIG. 12.— Comparison between source catalogs. Red squares are the results for the total sample (the same with Figure 11). Green circles show the results for AGNs which are selected by uniform criteria of SDSS (Richards et al. 2002) among the samples from the catalog of Shen et al. (2011). Blue triangles show the results for the AGN samples extracted from the catalog of Greene & Ho (2007).

ground and background galaxies but they should make no contribution to the clustering signal and not affect r_0 . For these analysis, we selected AGN samples with $M_{\text{th}} \equiv m_{\text{th}} - DM > -22.0$ and $M_{\text{th}} > -23.5$, respectively (see also Figure 3). Therefore, these absolute magnitude limited galaxy samples are also “complete” ($m < m_{\text{th}}$). Although the error bar is relatively large, we can see the similar trend of the cross correlation length against virial mass of SMBH as Figure 11. Significance of the difference of r_0 by considering statistical error is 1.9σ for mass ranges between $\log(M_{\text{BH}}/M_{\odot}) = 7.5-8.2$ and $8.2-9.0$, and 1.7σ for between $8.2-9.0$ and $9.0-10.0$, for the

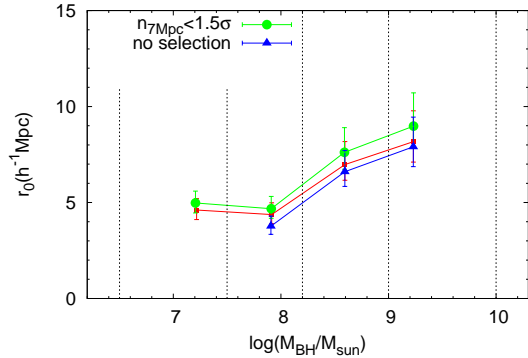


FIG. 13.— The scale length r_0 of cross-correlation for different selection criteria for AGN samples. *Blue triangles*: Results of the analysis without any sample rejection. *Red squares*: AGN samples with extremely inhomogeneous galaxy distribution around them are rejected by the criteria described in Shirasaki et al. (2011) in order to reduce the effect of foreground clusters which are accidentally located near the sample AGNs on the sky. The same with Figure 11. *Green circles*: Samples with extremely high or low ($> 1.5\sigma$) projected number density of galaxies $n_{7\text{Mpc}}$ is rejected. See also Section 2. Slightly larger r_0 is estimated for the analysis with the additional selection. On the other hand, the all analysis gives almost same relative mass dependence.

analysis with $M < -23.5$ sample, and 3.8σ for between $\log(M_{\text{BH}}/M_{\odot}) = 7.5-8.2$ and $8.2-9.0$ for the $M < -22.0$ sample. Therefore, we can conclude that the increase of the cross correlation length seen in the Figure 11 is not only due to the bias related with the galaxy brightness. The estimated scale length is larger than Figure 11 since blighter galaxies are more strongly clustered.

5. DISCUSSION

In the previous studies, Shen et al. (2009) have shown that most massive SMBHs are more strongly clustered than the remainders from auto-correlation analysis of quasars. It has also been shown that radio selected AGNs are strongly clustered than the cases for the optically selected AGNs (Hickox et al. 2009; Donoso et al. 2010), and characteristic BH mass of radio AGNs is higher than optically selected ones. Our results are consistent with these previous studies. These may indicate that the environment of galaxies has played an important role for the growth of high mass SMBHs. The clustering amplitude is relevant to the mass of the host dark-matter halo and the frequency of major merger. If mass growth of SMBH is mainly driven by the major mergers of galaxies, massive SMBHs are expected to be in massive halos.

In contrast, we did not found significant luminosity dependence. Luminosity is thought to represent gas accretion activity at this time. Activity of SMBH is thought to be a transient event and not strongly correlate with large scale structure. On the other hand, black hole mass is thought to represent cumulative accretion history and merger history of BHs, and can be related with large scale environment.

For less massive BHs with $M_{\text{BH}} \lesssim 10^8 M_{\odot}$, the significant correlation between r_0 and M_{BH} is not seen in our study. BH mass has been thought to be correlated with the mass of dark matter halo (e.g. Ferrarese 2002). Recently, however, Kormendy & Bender (2011) found that the mass of SMBH does not directly correlate with dark matter halo mass, at least for low-mass SMBHs in disk galaxies, based on the observations of nearby SMBHs for

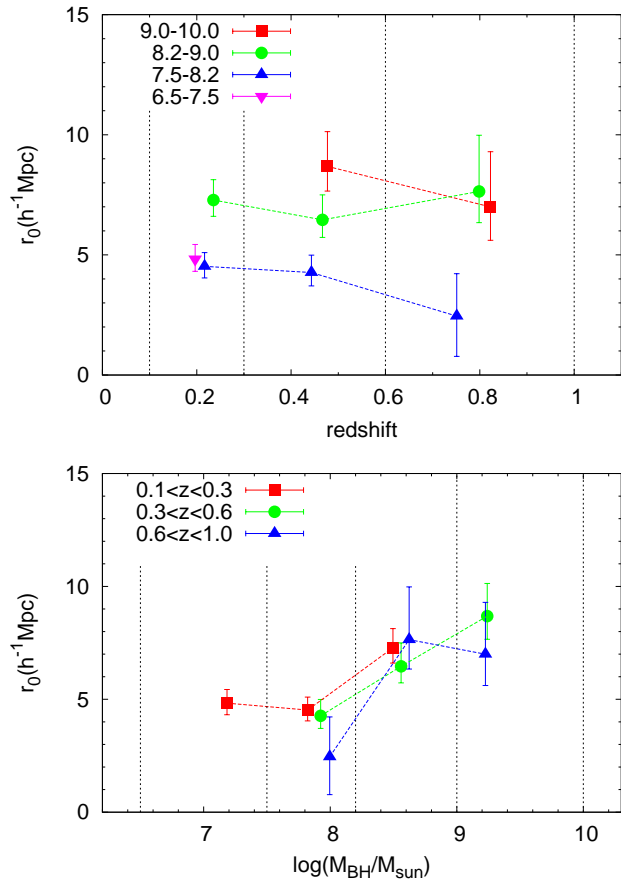


FIG. 14.— *Top panel*: The correlation length (r_0) against redshift for the samples of four BH mass ranges: $\log(M_{\text{BH}}/M_{\odot}) = 9.0-10.0$ (red squares), $8.2-9.0$ (green circles), $7.5-8.2$ (blue triangles), and $6.5-7.5$ (magenta inverted triangles). Results of mass and redshift range with $n_{\text{AGN}} < 200$ are not plotted because of very large uncertainty. Vertical dotted lines show boundaries of redshift ranges. *Bottom panel*: r_0 against BH mass for the samples of three redshift ranges: $z = 0.1-0.3$ (red squares), $z = 0.3-0.6$ (green circles), and $z = 0.6-1.0$ (blue triangles).

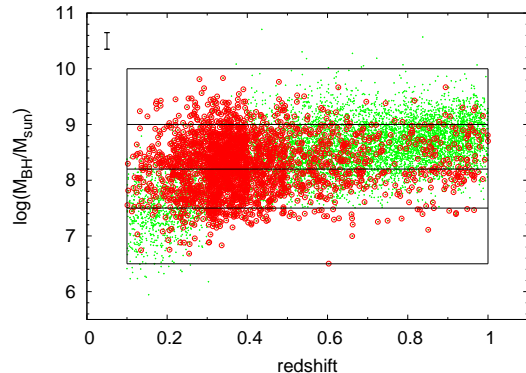


FIG. 15.— Resampling of the AGN sample in order to cancel the redshift dependence of the BH mass. The green crosses are the original sample (shown in Figure 6) and the red circles denote one set of the resampled AGNs. Selection probability is determined to give the same redshift distribution for the four mass ranges. We construct ten sets of the resampled AGNs by the Monte-Carlo method.

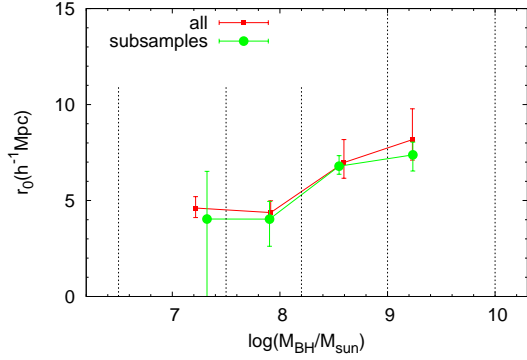


FIG. 16.— The scale length r_0 of cross-correlation against BH mass for the resampled AGNs (green circles). The sub-samples is selected to cancel the redshift dependence of the BH mass. Symbols show median, and error bars show maximum and minimum of the ten sample sets constructed by the Monte-Carlo resampling. We see the similar trend as the analysis for the all sample AGNs (red squares).

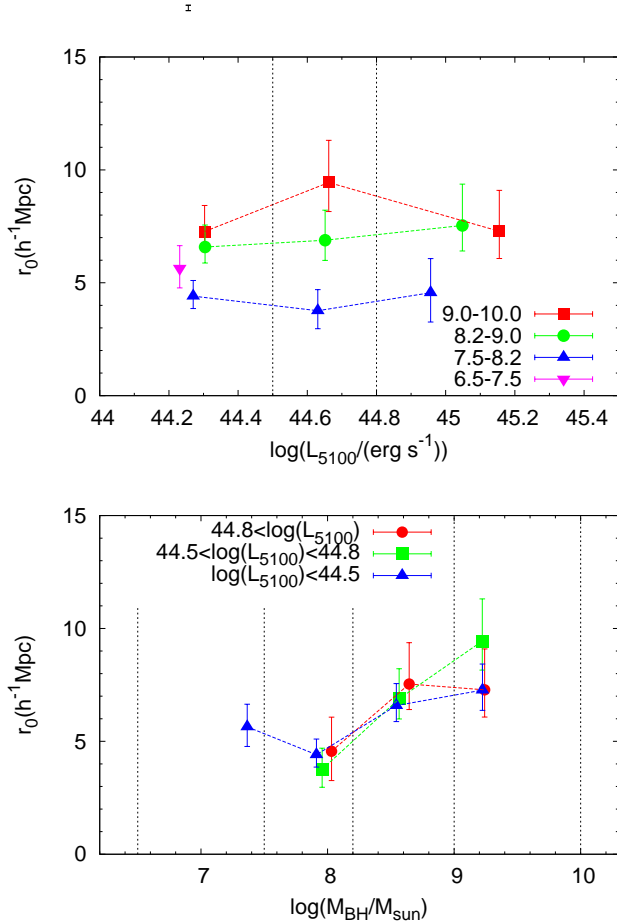


FIG. 17.— *Top panel:* The scale length (r_0) of cross-correlation against luminosity for the samples of four BH mass ranges: $\log(M_{\text{BH}}/M_{\odot}) = 9.0\text{--}10.0$ (red squares), $8.2\text{--}9.0$ (green circles), $7.5\text{--}8.2$ (blue triangles), and $6.5\text{--}7.5$ (magenta inverted triangles). *Bottom panel:* r_0 against BH mass for the samples of three luminosity ranges: $L_{5100} \geq 10^{44.8}\text{ erg/s}$ (red circles), $10^{44.5}\text{ erg/s} \leq L_{5100} < 10^{44.8}\text{ erg/s}$ (green squares), and $L_{5100} < 10^{44.5}\text{ erg/s}$ (blue triangles).

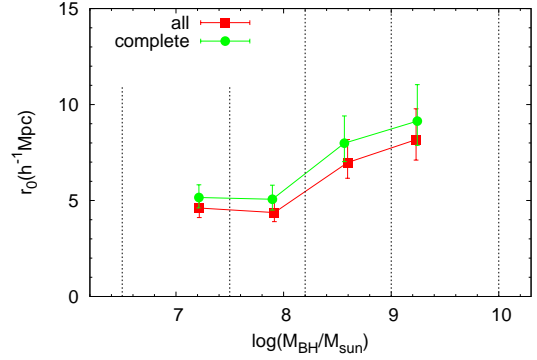


FIG. 18.— The cross correlation length for complete galaxy sample as a function of virial mass of SMBH. The complete sample is galaxy samples which is blighter than threshold magnitude m_{th} for each region around AGN. (See also Section 3)

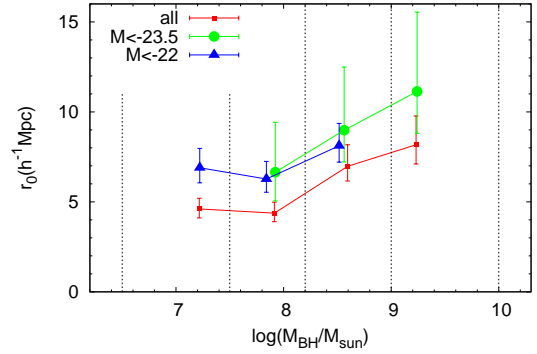


FIG. 19.— The cross correlation length for luminosity limited galaxy samples as a function of virial mass of SMBH. The luminosity limited samples are defined as $M \equiv m - DM(z_{\text{AGN}}) < -22.0$ (blue triangle) and $M < -23.5$ (green circle), respectively. Where $DM(z_{\text{AGN}})$ represents distance modulus for the AGN redshift z_{AGN}

which mass of the host dark halos are derived by the stellar kinematics.

One possible scenario to explain the absence of the positive mass dependence for $M_{\text{BH}} \lesssim 10^8 M_{\odot}$ would be that the less massive BHs could be formed in the isolated galaxies by secular processes. If they have grown by secular processes, mass of a seed BH should be much larger than a typical stellar mass BH (for a review, see, e.g., Volonteri 2010). Some authors (Lodato & Natarajan 2006; Begelman et al. 2006) argue that SMBHs with $10^4\text{--}10^6 M_{\odot}$ are formed through the direct collapse of pre-galactic gas at $z > 10$. Such a heavy seed BH can grow to $\sim 10^7\text{--}10^8 M_{\odot}$ by a few Gyrs without BH merger under the assumption that the mass accretion rate is around ~ 0.1 times the Eddington rate. Another scenario would be that they are in a growing phase by the major mergers of galaxies.

For the clustering amplitude of less massive SMBHs, the contribution of the AGNs hosted in satellite galaxies in the massive dark-matter halos can also be important, while most massive SMBHs are in the central regions of dark-matter halos. Padmanabhan et al. (2009) argue that the satellite fraction of quasars is more than 25% in their sample, which is selected from the SDSS catalog. The percentage should be larger for the less massive BHs. Further investigation of less massive BHs is crucial

to understand formation and evolution mechanisms of a SMBH.

6. CONCLUSIONS

We have investigated the clustering of galaxies around 9,394 AGNs for $z = 0.1-1$. We obtained the galaxy data of UKIDSS LAS by means of virtual observatory tools. Our results are free from the effect of cosmic variance owing to the large sample covering the large area of the sky. The estimated correlation length ranges between $4-10h^{-1}\text{Mpc}$ depending on BH mass, and depends neither on redshift for $z = 0.1-1$ nor on luminosity. The results may indicate that higher mass BHs reside in more clustered environment for $M_{\text{BH}} > 10^8 M_{\odot}$.

While our results show positive mass dependence for $M_{\text{BH}} > 10^8 M_{\odot}$, our results for $M_{\text{BH}} \lesssim 10^8 M_{\odot}$ show no significant mass dependence. Although our sample of less massive BHs is small, this would give a critical mass scale for emergence of environment effect for BH growth.

In this study the redshift range where the BH mass dependence of the cross correlation is measured with good accuracy is limited to below $z \sim 0.6$. This is because the number density of UKIDSS LAS galaxies is too low at higher redshift, and also the systematic error due to the uncertainty of M_* parameter of luminosity function is too large. To understand the relation of the BH mass accretion history and its environment, it is crucial to observe its evolution upto at least redshift two where the number density of QSO is maximal and the mass accretion is expected to be the most prosperous. To reduce the uncertainty, it is crucial to perform deeper observations so that the limiting magnitude reaches well beyond the characteristic luminosity of galaxies

at AGN redshifts. At redshifts larger than 0.5, the dominant factor to the uncertainty of ρ_0 is uncertainty of M_* parameterization and the ρ_0 uncertainty becomes larger than 20%. Two magnitude deeper observation will extend the redshift range where the uncertainty of ρ_0 is less than 20% up to 1.0. Future instruments such as Hyper Suprime-Cam (HSC) can measure the AGN environment more accurately with good statistics. When the survey is performed with 26 mag in r band with HSC, we can estimate ρ_0 with accuracy less than 20% up to redshift 2, and as a result can estimate r_0 with accuracy less than 10%. Such a deep and wide survey would reveal the mechanism of AGN evolution at an important epoch that its activity was the most prosperous.

We appreciate to S. Eguchi and M. Enoki for their useful discussions. Results are based on data obtained from the Japanese Virtual Observatory, which is operated by the Astronomy Data Center, National Astronomical Observatory of Japan. This research has made use of the VizieR catalogue access tool, CDS, Strasbourg, France. This work is based on data obtained as part of the UKIRT Infrared Deep Survey. Funding for the SDSS and SDSS-II has been provided by the Alfred P. Sloan Foundation, the Participating Institutions, the National Science Foundation, the U.S. Department of Energy, the National Aeronautics and Space Administration, the Japanese Monbukagakusho, the Max Planck Society, and the Higher Education Funding Council for England. The SDSS Web Site is <http://www.sdss.org/>.

REFERENCES

- Barr, J. M., Bremer, M. N., Baker, J. C., & Lehnert, M. D. 2003, MNRAS, 346, 229
 Begelman, M. C., Volonteri, M., & Rees, M. 2006, MNRAS, 370, 289
 Cirasuolo, M. et al. 2007, MNRAS, 380, 585
 Coil, A. L. et al. 2009, ApJ, 701, 1484
 Donoso, E., Li, C., Kauffmann, G., Best, P. N., & Heckman, T. M. 2010, MNRAS, 407, 1078
 Ferrarese, L., & Ford, H. 2005, SSRv, 116, 523
 Ferrarese, L., & Merritt, D. 2000, ApJ, 539, L9
 Ferrarese, L. 2002, ApJ, 578, 90
 Gabasch, A. et al., 2004, A&A, 421, 41
 Gabasch, A. et al., 2006, A&A, 448, 101
 Greene, J. E., & Ho, L. C. 2007, ApJ, 670, 92
 Hickox et al. 2009, ApJ, 696, 891
 Kochanek, C. S. et al., 2001, ApJ, 560, 566
 Kormendy, J., & Bender, R., 2011, Nature, 469, 377
 Krumpe, M., Miyaji, T., Coil, A. L., & Aceves, H., 2012, ApJ, 746, 1
 Lawrence et al. 2012, yCat, 2314
 Lodato, G. & Natarajan, P. 2006, MNRAS, 371, 1813
 Magorrian, J., et al. 1998, AJ, 115, 2285
 Montero-Dorta, A. D. & Prada, F., 2009, MNRAS, 399, 1106
 Mountrichas, G., Sawangwit, U., Shanks, T., Croom, S. M., Schneider, D. P., Myers, A. D., & Pimblet, K. 2009, MNRAS, 394, 2050
 Padmanabhan, N., White, M., Norberg, P., and Porciani, C. 2009, MNRAS, 397, 1862
 Richards et al. 2002, AJ, 123, 2945
 Richstone, D., et al. 1998, Nature, 395, 14
 Ross et al. 2009, ApJ, 697, 1634
 Schneider, D. P., et al. 2010, ApJ, 139, 2360
 Shen, Y., et al. 2007, AJ, 133, 2222
 Shen, Y., et al. 2009, ApJ, 697, 1656
 Shen, Y., et al. 2011, ApJS, 194, 45
 Shirasaki, Y., Tanaka, M., Ohishi, M., Mizumoto, Y., Yasuda, N., & Takata, T. 2011, PASJ, 63, 469
 Volonteri, M. 2010, A&ARv. 18, 279

TABLE 1
STATISTICS OF FITTING PARAMETERS FOR EACH VIRIAL MASS AND REDSHIFT GROUP

| virial mass $\log(M_{\text{BH}}/M_{\odot})$ | redshift | $n_{\text{AGN}}^{\text{a}}$ | $\langle \log(M_{\text{BH}}/M_{\odot}) \rangle^{\text{b}}$ | $\langle z \rangle^{\text{c}}$ | r_0^{d} $h^{-1}\text{Mpc}$ | n_{bg}^{e} Mpc^{-2} | $\langle \rho_0 \rangle^{\text{f}}$ 10^{-3}Mpc^{-3} |
|--|----------|-----------------------------|--|--------------------------------|--|---|---|
| all | 0.1–1.0 | 9394 | 8.42 | 0.59 | $5.8^{+0.8}_{-0.6}$ | 10.473 ± 0.005 | 1.9 ± 0.4 |
| 9.0–10.0 | 0.1–1.0 | 1331 | 9.23 | 0.72 | $8.2^{+1.6}_{-1.1}$ | 4.542 ± 0.008 | 0.93 ± 0.25 |
| | 0.1–0.3 | 33 | 9.27 | 0.24 | – ^g | – | – |
| | 0.3–0.6 | 347 | 9.24 | 0.48 | $8.7^{+1.4}_{-1.0}$ | 7.29 ± 0.02 | 2.0 ± 0.5 |
| | 0.6–1.0 | 951 | 9.22 | 0.82 | $7.0^{+4.9}_{-2.1}$ | 2.70 ± 0.01 | 0.38 ± 0.15 |
| 8.2–9.0 | 0.1–1.0 | 5119 | 8.60 | 0.66 | $7.0^{+1.2}_{-0.8}$ | 6.001 ± 0.005 | 1.3 ± 0.3 |
| | 0.1–0.3 | 320 | 8.50 | 0.24 | $7.3^{+0.9}_{-0.7}$ | 29.40 ± 0.04 | 5.3 ± 0.9 |
| | 0.3–0.6 | 1635 | 8.56 | 0.47 | $6.5^{+1.0}_{-0.7}$ | 7.49 ± 0.01 | 2.1 ± 0.5 |
| | 0.6–1.0 | 3164 | 8.62 | 0.80 | $7.6^{+2.3}_{-1.3}$ | 2.87 ± 0.004 | 0.42 ± 0.16 |
| 7.5–8.2 | 0.1–1.0 | 2278 | 7.91 | 0.44 | $4.4^{+0.6}_{-0.5}$ | 15.69 ± 0.01 | 2.8 ± 0.6 |
| | 0.1–0.3 | 664 | 7.82 | 0.22 | $4.5^{+0.6}_{-0.5}$ | 38.26 ± 0.03 | 5.7 ± 1.0 |
| | 0.3–0.6 | 967 | 7.92 | 0.44 | $4.3^{+0.7}_{-0.6}$ | 8.53 ± 0.01 | 2.3 ± 0.5 |
| | 0.6–1.0 | 642 | 8.00 | 0.75 | $2.5^{+1.8}_{-1.7}$ | 3.22 ± 0.01 | 0.53 ± 0.19 |
| 6.5–7.5 | 0.1–1.0 | 635 | 7.22 | 0.25 | $4.6^{+0.6}_{-0.5}$ | 38.65 ± 0.03 | 5.4 ± 0.9 |
| | 0.1–0.3 | 513 | 7.18 | 0.20 | $4.8^{+0.6}_{-0.5}$ | 45.69 ± 0.04 | 6.1 ± 1.0 |
| | 0.3–0.6 | 101 | 7.36 | 0.38 | – | – | – |
| | 0.6–1.0 | 21 | 7.30 | 0.77 | – | – | – |

^anumber of sample AGNs

^baverage of logarithm of BH mass

^caverage redshift

^dcorrelation length, the error contains the systematic error due to the uncertainty of ρ_0 and the 1σ statistical error.

^eaverage of the projected number density of background galaxies

^faverage of the averaged number density of galaxies at the AGN redshift

^gWe do not derive parameters for sub-sample with $n_{\text{AGN}} < 200$